PROCEEDINGS OF SCIENCE

Calibration strategy of the ASTRI Mini-Array Cherenkov cameras

Davide Mollica,[a,*] **Osvaldo Catalano,**[a] **Giovanni Contino,**[a] **Milvia Capalbi,**[a] **Mattia Corpora,**[a] **Fabio Paolo Lo Gerfo,**[a] **Pierluca Sangiorgi,**[a] **Giuseppe Sottile,**[a] **Simone Iovenitti,**[b] **Giuseppe Leto,**[c] **Teresa Mineo,**[a] **Salvatore Scuderi,**[d] **Gino Tosti**[e] **and Giovanni Pareschi**[b] **for the ASTRI Project**

[a] *INAF, Istituto di Astrofisica Spaziale e Fisica Cosmica, Via Ugo la Malfa 153, I-90146 Palermo, Italy*
[b] *INAF, Osservatorio Astronomico di Brera, Via Brera 28, I-20121 Milano, Italy*
[c] *INAF, Osservatorio Astronomico di Catania, Via Santa Sofia 78, I-95123 Catania, Italy*
[d] *INAF, Istituto di Astrofisica Spaziale e Fisica Cosmica, Via Alfonso Corti 12, I-20133 Milano, Italy*
[e] *Dipartimento di Fisica, Università degli Studi di Perugia, I-06123 Perugia, Italy*

E-mail: davide.mollica@inaf.it

The ASTRI Mini-Array is an international project led by the Italian National Institute for Astrophysics (INAF) to deploy an array of nine Imaging Atmospheric Cherenkov Telescopes at the Teide Observatory in Tenerife. The system will study astronomical sources emitting at very high-energy above 1 TeV. The telescopes are an improved version of the ASTRI-Horn telescope (Mt. Etna, Italy), a 4-m diameter prototype developed by INAF in the context of the ASTRI Project.
The novel Mini-Array Cherenkov camera, based on Silicon Photo-Multiplier (SiPM) detectors, is an evolution of the ASTRI-Horn telescope camera. The camera focal plane is equipped with 2368 SiPM pixels with dimensions of 7 mm × 7 mm arranged in tiles of 8 × 8 pixels. Each tile together with the ASIC board and the FPGA board constitutes a Photon Detection Module (PDM). 37 PDMs are arranged to match the spherical profile of the focal surface.
In this contribution we present the camera calibration strategy and tools developed thanks to the experience gained with the ASTRI-Horn telescope. These calibration procedures are essential tasks to extract SiPMs calibration coefficients, which are needed for the Cherenkov data analysis, and camera configuration parameters that ensure system stability and a uniform trigger efficiency over the whole telescope field of view. Moreover, these procedures allow to monitor the system performance and health during the data taking.

38th International Cosmic Ray Conference (ICRC2023)
26 July - 3 August, 2023
Nagoya, Japan

*Speaker

PoS(ICRC2023)765

1. Introduction

The ASTRI Mini-Array [1] is designed to study astronomical sources emitting at very high-energy (VHE) in the 1 TeV-200 TeV energy band. The array will consist of nine small-sized (4-m diameter) and large field of view (10.5°) Imaging Atmospheric Cherenkov Telescopes (IACTs) under deployment at the *Observatorio del Teide* (Tenerife, Spain). The array telescopes have a dual-mirror Schwarzschild-Couder optical design characterized by a small plate-scale (about 37.5 mm/deg), allowing the use of Silicon Photo-Multiplier (SiPM) detectors. In order to ensure data acquisition consistency and to extract parameters from air-shower images, it is essential to keep the acquisition system stable, monitor its health status, make the trigger efficiency uniform and accurately calibrate SiPMs and electronics.

The most important calibration procedures, described in section 3, are based on procedures developed for the ASTRI-Horn telescope [2] (therefore they are fully compatible with the new cameras) and have been successfully tested and applied on prototype data. These set of calibration procedures will be applied for calibration and monitoring of the ASTRI Mini-Array Cherenkov cameras, starting with the commissioning of the first telescope (ASTRI-1), scheduled to begin in fall 2023, and the first stereo system consisting of the first three telescopes (ASTRI-1, ASTRI-8, ASTRI-9), scheduled to begin in the first half of 2024 [3].

The preliminary measurements presented in the next section have been performed in lab during the assembly of the new hardware and the development of the new firmware.

2. The ASTRI Cherenkov camera

The ASTRI Mini-Array camera [4] is an evolution of the ASTRI-Horn camera [5]. It is based on SiPM detectors organized in 37 Photon Detection Modules (PDMs) each of 8×8 pixels, with a total of 2368 pixels each with dimensions of 7 mm×7 mm.

A PDM contains the SiPM tile (Hamamatsu S14521), the Front End Electronics (FEE) and a Field Programmable Gate Array (FPGA). The SiPMs signal is processed by the FEE, which consists of two 32-channels CITIROC-1A ASICs [6, 7]. Each channel has two separated processing chains, High-Gain (HG) and Low-Gain (LG), with different gain configuration and shaped with the same, programmable, shaping time (25 ns by default). Both chains have a Peak Detector (PD) that measures the maximum height of the shaped signal.

A bipolar fast-shaper (15 ns shaping time) is connected to the HG that, in turn, is connected to a discriminator with a 10 bit programmable threshold (the same for all 32 channels of each ASIC) that provides a digital trigger signal. The Xilinx Artix 7 FPGA controls the generation of a *PDM trigger* (when a certain condition on trigger channels is fulfilled) that is sent to the back-end electronics that provides the *camera trigger* signal to all PDMs. At the occurrence of a camera trigger, the PD is armed and, after an appropriate delay (that depends on the peaking time), HG and LG pulse height digitization is performed.

Signal variance The *variance technique* is the measurement of the dispersion of the HG and LG signal generated by each pixel. The AC-coupled readout electronics keeps the baselines of the ADC converters stable at a default value. Therefore, when SiPMs are exposed to slow-varying Poisson source, the induced HG and LG signals will have a fixed average value independent of source

rate, but with a variance value that is linearly proportional to it (see section 3.2). The variance is computed by the FPGA sampling both HG and LG signals continuously without interfering with the Cherenkov data acquisition.

Internal calibration system The ASTRI camera is equipped with an ancillary calibration device, the Fiber-Optic Calibration (FOC), that can operate in dark condition (i.e. when the camera lids are closed). The FOC is composed of two laser diodes (green and blue) coupled with a fiber optic cable placed on the edge of the filter window of the camera. In this way, the light propagates through the fiber into the filter window and eventually reaches the focal plane illuminating all the SiPMs surface. The light emitted by laser diodes can be pulsed or continuous, allowing to perform on-site all the calibration procedures described in the next section.

3. Relative calibration

The SiPM micro-cell gain G is the number of electrons produced in an electron avalanche initiated by a photon or by thermal excitation:

$$G = \frac{Q_{\text{tot}}}{e} = \frac{C}{e}\left(V_{\text{op}} - V_{\text{br}}\right), \tag{1}$$

where Q_{tot} is the generated total charge, e is the elementary charge, C is the single micro-cell capacitance, V_{op} is the operating voltage and V_{br} is the SiPM breakdown voltage. The factor $V_{\text{ov}} = V_{\text{op}} - V_{\text{br}}$ is called *over-voltage*.

Since the V_{op} is shared by all 64 pixels of each PDM, small gain differences are expected. Moreover, non-uniformity could be introduced by the FEE. The relative calibration aims to equalize and stabilize the response of HG, LG and trigger chains and to provide all the calibration coefficients needed for the Cherenkov data analysis [8].

3.1 Temperature compensation

The breakdown voltage is a characteristic of the SiPM and depends on temperature. Since the temperature dependence of the micro-cells capacity can be neglected [9], the gain dependence on temperature is

$$\frac{\partial G}{\partial T} = \frac{C}{e}\frac{\mathrm{d}V_{\text{br}}}{\mathrm{d}T}. \tag{2}$$

The temperature-induced shift of V_{br} affects also the most critical characteristics of SiPMs: cross-talk probability and photon detection efficiency. In order to mitigate the variation of those parameters, it is indispensable to perform the so called *temperature compensation*. Indeed, according to equation 1, the gain does not depend on temperature if the over-voltage is fixed. If one knows how V_{br} varies with temperature, the over-voltage can be kept constant varying the operating voltage accordingly. Since the dependence on temperature of the V_{br} of UV-sensitive SiPM can be linearized around an operational temperature T_0 [9–11], the temperature compensation can be written as

$$V_{\text{op}}(T) = V_{\text{br}}(T) + V_{\text{ov}} = V_{\text{br},0} + (T - T_0)\,\frac{\mathrm{d}V_{\text{br}}}{\mathrm{d}T} + V_{\text{ov}}. \tag{3}$$

The compensation is fully determined by the breakdown voltage $V_{\text{br},0}$ at the reference temperature T_0 and by the slope $\mathrm{d}V_{\text{br}}/\mathrm{d}T$.

3.2 Breakdown voltage determination

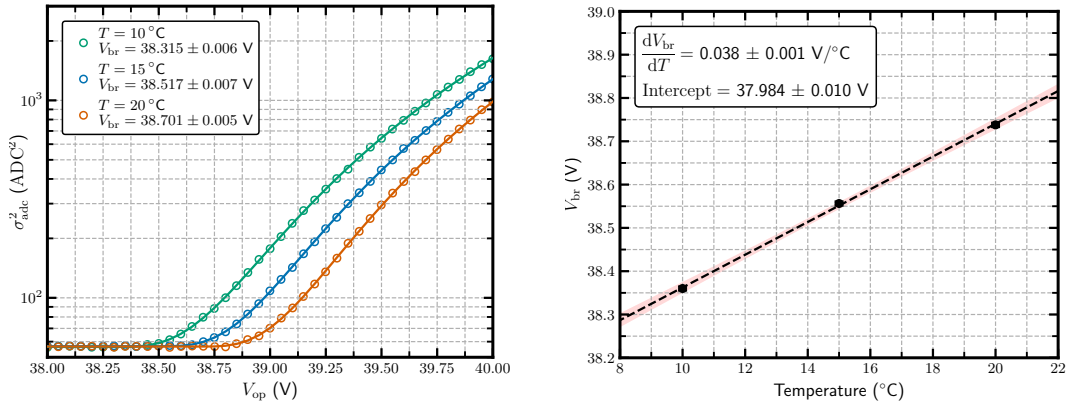

Figure 1: Left) VAR-V curve for a single SiPM at three different temperatures. The solid lines are the result of the fits with the function 7. Right) Average V_{br} derived from the VAR-V curves of all 64 pixels of a PDM as a function of temperature. The dashed curve is the best fit with a linear model. The filled area is a 3σ confidence band.

The breakdown voltage is obtained by measuring the output current as a function of the reverse voltage of the SiPM, the so-called I-V curve. The most common method of evaluating V_{br} uses a stable light source that illuminates the SiPM pixels at various applied voltages and reads the individual SiPM pixel current using a source meter directly connected to the SiPM. This method is very efficient but the setup requires an external instrument such as a picoammeter and in the case of a large number of SiPM pixels the measurement is time-consuming. The novel method we adopt to derive V_{br} consists in measuring the signal variance as a function of the reverse voltage (VAR-V curve), using as well a stable light source for illuminating pixels. Advantages of this method is quite obvious: its applicability is straightforward and essentially requires no tools beyond the camera graphical user interface from which the VAR-V measurement is performed. If we illuminate the SiPM with a Poissonian light source with average rate ϕ_{source}, the mean current value is proportional to the photons rate

$$\langle I \rangle \propto \phi_{\mathrm{source}}. \tag{4}$$

Assuming a generalized Poisson distribution due to cross-talk contribution [12], the induced photo-electron rate can be written as

$$\phi^{\mathrm{pe}}_{\mathrm{source}} \propto \frac{\sigma^2_{\mathrm{source}}}{(1-\lambda)^3} P_{\mathrm{br}}, \tag{5}$$

where P_{br} is the breakdown probability, λ is the Borel parameter (that is approximately the cross-talk probability) and $\sigma^2_{\mathrm{source}}$ is the variance of the source (i.e. the mean photon rate). The variance of the digitally converted signal is

$$\sigma^2_{\mathrm{adc}} \propto \bar{g}^2 \phi^{\mathrm{pe}}_{\mathrm{source}} \propto \bar{g}^2 \frac{\phi_{\mathrm{source}}}{(1-\lambda)^3} P_{\mathrm{br}}, \tag{6}$$

where $\bar{g}$ is the pixel gain in ADC unit (see section 3.4). Therefore, the current is proportional to the variance of the signal. If we describe each term of the relation 6 by their bias voltage dependency [9], finally we get the parameterized VAR-V relation

$$\sigma^2_{\text{adc}}\left(V_{\text{op}}\right) = \begin{cases} \sigma_0^2 & \text{if } V_{\text{op}} < V_{\text{br}}, \\ \sigma_0^2 + \beta \dfrac{V_{\text{ov}}^2\left(1 - \mathrm{e}^{-\frac{V_{\text{ov}}}{\alpha}}\right)}{\left(1 - \gamma V_{\text{ov}}\left(1 - \mathrm{e}^{-\frac{V_{\text{ov}}}{\alpha}}\right)\right)^3} & \text{if } V_{\text{op}} > V_{\text{br}}, \end{cases} \tag{7}$$

where:

- σ_0^2 is the signal variance due to leakage current and electronic noise;
- β is a proportionality factor that depends on the readout electronics, micro-cells capacitance and light source intensity;
- γ describes the linear relation between V_{ov} and the number of discharge-induced photons that can generate a cross-talk discharge;
- α describes how fast the breakdown probability raises with the over-voltage.

Preliminary measurements of the breakdown voltage at different temperatures using VAR-V curves are shown in figure 1 (left). The right panel of the same figure shows a preliminary determination of the V_{br} temperature dependence needed to apply the temperature compensation.

3.3 Trigger channels alignment

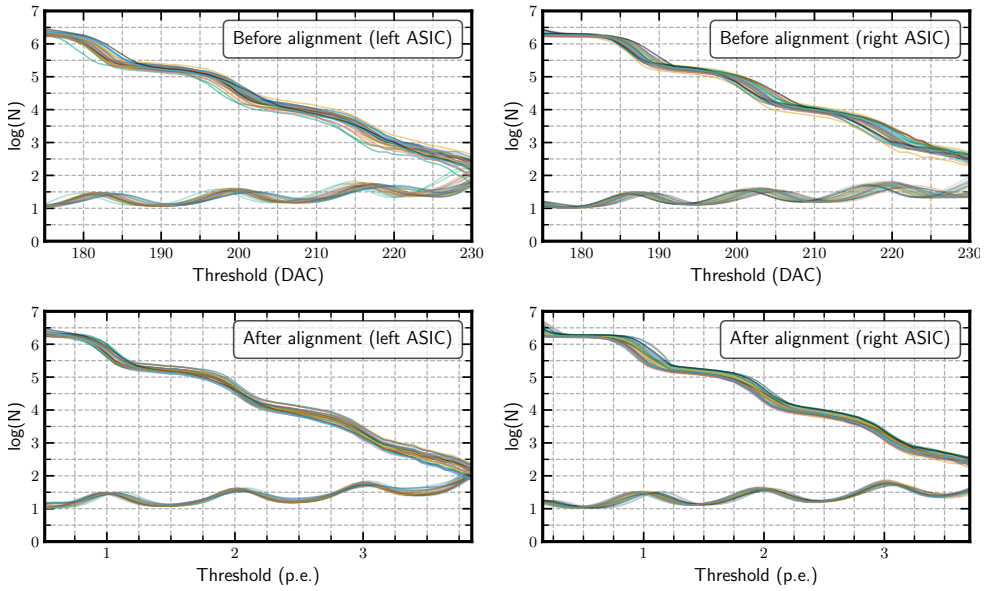

Figure 2: Trigger alignment procedure of both ASICs (left and right) of a PDM. Top) Staircase curves of all channels before the alignment. Bottom) Staircase plot after the threshold correction (see equation 8) computed to align channels to the third photo-electron. The log-derivative at the bottom of the plots is shown for visualization purpose.

First level trigger signals equalization is of fundamental importance for carrying out an effective and robust relative calibration of the camera. As the first level trigger signals are at the base of the acquisition of the physical event, trigger equalization and hence stability are essential for a correct and reliable camera operation. As for any multi-channel front-end electronics, small differences

between trigger channels are expected. The causes of such non-uniformity are numerous although usually small differences in voltage reference of the discriminators are the main issue.

The trigger alignment and the threshold calibration are performed by counting, in dark condition, the total number of spontaneous trigger signals per pixel as a function of the threshold voltage (known as *staircase* curve). Staircase plots for both ASICs of a PDM are show in figure 2 (top). From curves inflection points is possible to locate the positions, in DAC unit, of each photo-electron. The DAC threshold is shared between the 32 ASIC channels. Possible misalignments can be corrected by means of a programmable 4 bit DAC which slightly modifies channel discriminator reference voltage. If Δ^i_{4bit} is the DAC shift per DAC-4 bit value of the channel i, the values needed to align ASIC channels to the n-th photo-electron are

$$\epsilon^i_{\text{4bit}} = \frac{\left(x^{\text{pivot},n}_{\text{DAC}} - x^{i,n}_{\text{DAC}}\right)}{\Delta^i_{\text{4bit}}}, \tag{8}$$

where $x^{\text{pivot},n}_{\text{DAC}}$ is the n-th photo-electron position to which align other channels. The pivot channel is chosen in such a way to maximize the number of alignable channels. The DAC-pe conversion is performed measuring the mean distance between staircase inflection points Δ^i_{peq} of each channel

$$x_{\text{pe}} = 1 + \frac{x_{\text{DAC}} - \langle x^{i,1}_{\text{DAC}} \rangle}{\langle \Delta^i_{\text{peq}} \rangle}. \tag{9}$$

A preliminary alignement, to the third photo-electron, and calibration of the trigger chain of a PDM is shown in figure 2 (bottom).

3.4 Relative gain calibration from pulse-height distributions

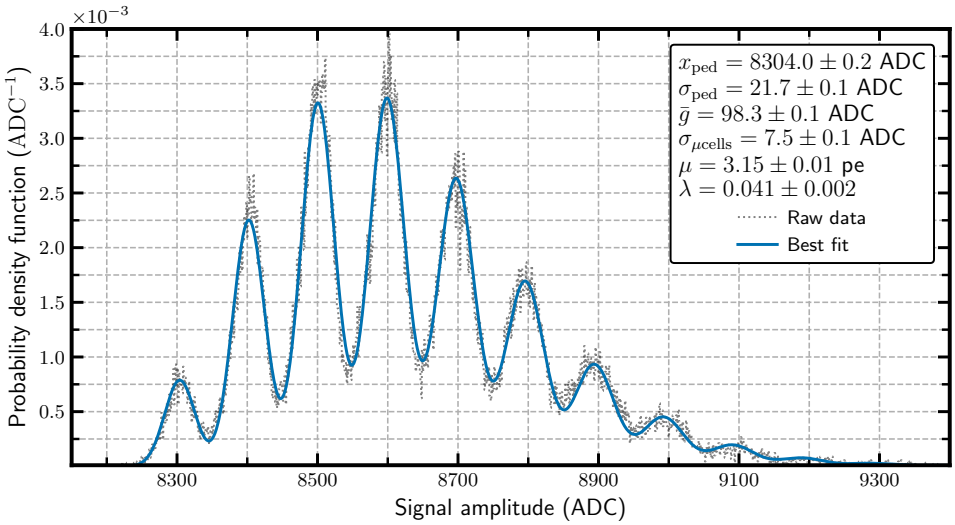

Figure 3: Relative gain calibration of a SiPM illuminated by a pulsed light source using the pulse-height differential distribution. The dotted line is the raw data, the solid line is the best-fit with a Gaussian-smeared general Poisson distribution (see equation 10).

The Pulse-Height Distribution (PHD) of each SiPM is obtained illuminating the focal plane with short light flashes with a pulse duration of about 10 ns and with a constant frequency of 500 Hz.

Assuming a Poisson distribution with mean value μ photo-electrons for each flash and a Borel branching process with parameter λ for the number of photo-electrons due to cross-talk discharges, the expected photo-electron distribution is well described by a generalized Poisson distribution [12]

$$p_{\mathrm{GP}}(k,\mu,\lambda) = \frac{\mathrm{e}^{-\mu-\lambda k}\mu\,(\mu+\lambda k)^{k-1}}{k!}.$$

Taking into account the smearing due to electronic noise and the gain dispersion between micro-cells, the PHD, at a digitalized ADC value x_{adc}, can be expressed as a Gaussian-smeared generalized Poisson distribution [13]

$$f_{\mathrm{PHD}}(x_{\mathrm{adc}}) = \sum_{k=0}^{\infty} f_{\mathrm{G}}\left(x_{\mathrm{adc}},\ x_{\mathrm{ped}} + k\bar{g},\ \sqrt{\sigma^2_{\mathrm{ped}} + k\sigma^2_{\mu\mathrm{cells}}}\right) p_{\mathrm{GP}}(k,\mu,\lambda), \tag{10}$$

where:

- $f_{\mathrm{G}}(x,\mu,\sigma)$ is a normal probability density function with mean μ and standard deviation σ;
- x_{ped} and σ_{ped} are the pedestal position and dispersion (the electronic noise) in ADC;
- $\bar{g}$ is the *equivalent photo-electron* (the pixel micro-cells mean gain in ADC unit);
- λ is he mean number of Geiger discharges per photo-detection induced by cross-talk;
- $\sigma_{\mu\mathrm{cells}}$ is the photo-electron dispersion due to gain differences between pixel micro-cells.

An example of pixel characteristics extraction using the model 10 is shown in figure 3. The application of this calibration method to the ASTRI-Horn data has shown that the parameters reconstruction is reliable as long as the first photo-electron dispersion is lower than about $0.5\,\bar{g}$. This calibration procedure provides the necessary calibration coefficients needed to convert pixel signals from ADC counts to the number of photo-electrons:

$$x_{\mathrm{pe}} = \frac{x_{\mathrm{adc}} - x_{\mathrm{ped}}}{\bar{g}}, \quad \sigma^2_{\mathrm{pe}} = \frac{\sigma^2_{\mathrm{adc}}}{\bar{g}^2}. \tag{11}$$

The *cross-talk correction* is essential when calculating statistical estimators of the source signal, since allows to remove the excess noise factor of each SiPM. For example, recalling equation 6, to evaluate the rate of primary photo-electrons induced by night sky background photons

$$\phi^{\mathrm{pe}}_{\mathrm{NSB}} \propto \frac{\sigma^2_{\mathrm{adc}}}{\bar{g}^2}\,(1-\lambda)^3\,. \tag{12}$$

It is worth highlighting that the assumption of a branching Poisson process does not take into account the recovery time of fired micro-cells and thus overestimates the number of cross-talk discharges. Nevertheless, the effect is negligible if $\lambda \lesssim 0.25$ [13] and in low-light condition.

4. Conclusions

We have reported on the main calibration procedures required for ASTRI Mini-Array cameras. These procedures were tested in the laboratory using the ASTRI Mini-Array camera electronics chain and SiPMs and will be used to test the first fully-assembled camera during the commissioning phase of the ASTRI-1 telescope. Thanks to the calibration system embedded in the camera (see section 2), these procedures, implemented in the ASTRI Mini-Array calibration software [14], will

allow users to quickly monitor and extract periodically calibration parameters of each telescope camera. The methods and algorithms were successfully applied for on-site ASTRI-Horn camera calibration and the results are used in data analysis.

Acknowledgments

This work was conducted in the context of the ASTRI Project. We gratefully acknowledge support from the people, agencies, and organisations listed here: http://www.astri.inaf.it/en/library/. This paper went through the internal ASTRI review process.

References

[1] S. Scuderi et al., *The ASTRI Mini-Array of Cherenkov telescopes at the Observatorio del Teide*, *Journal of High Energy Astrophysics* **35** (2022) 52.

[2] G. Leto and et al, *Status and performance of the ASTRI-Horn dual mirror air-Cherenkov telescope after a major maintenance and refurbishment intervention*, in *Proc. 38th ICRC*, PoS(ICRC2023)729, (Nagoya, Japan), 2023.

[3] A. Giuliani et al., *Status of the ASTRI program: technology and science with wide-field aplanatic IACT telescopes*, in *Proc. 38th ICRC*, PoS(ICRC2023)892, (Nagoya, Japan), 2023.

[4] G. Sottile et al., *The ASTRI Cherenkov Camera: from the prototype to the industrial version for the Mini-Array*, 2023. 10.48550/arXiv.2301.09915.

[5] O. Catalano et al., *The ASTRI camera for the Cherenkov Telescope Array*, in *Ground-based and Airborne Instrumentation for Astronomy VII*, C.J. Evans, L. Simard and H. Takami, eds., vol. 10702, p. 1070237, International Society for Optics and Photonics, SPIE, 2018, DOI.

[6] D. Impiombato et al., *Characterization and performance of the ASIC (CITIROC) front-end of the ASTRI camera*, *Nuclear Instruments and Methods in Physics Research Section A: Accelerators, Spectrometers, Detectors and Associated Equipment* **794** (2015) 185.

[7] J. Fleury et al., *Petiroc and Citiroc: front-end ASICs for SiPM read-out and ToF applications*, *JINST* **9** (2014) C01049.

[8] M. Mastropietro et al., *The ASTRI Mini-Array Cherenkov Data Pipeline*, in *Proc. 38th ICRC*, PoS(ICRC2023)765, (Nagoya, Japan), 2023.

[9] A.N. Otte et al., *Characterization of three high efficiency and blue sensitive silicon photomultipliers*, *Nuclear Instruments and Methods in Physics Research Section A: Accelerators, Spectrometers, Detectors and Associated Equipment* **846** (2017) 106.

[10] M. Ramilli, *Characterization of SiPM: Temperature dependencies*, in *2008 IEEE Nuclear Science Symposium Conference Record*, pp. 2467–2470, 2008, DOI.

[11] N. Serra et al., *Experimental and TCAD Study of Breakdown Voltage Temperature Behavior in n^+/p SiPMs*, *IEEE Transactions on Nuclear Science* **58** (2011) 1233.

[12] S. Vinogradov, *Analytical models of probability distribution and excess noise factor of solid state photomultiplier signals with crosstalk*, *Nuclear Instruments and Methods in Physics Research Section A: Accelerators, Spectrometers, Detectors and Associated Equipment* **695** (2012) 247.

[13] V. Chmill et al., *On the characterisation of SiPMs from pulse-height spectra*, *Nuclear Instruments and Methods in Physics Research Section A: Accelerators, Spectrometers, Detectors and Associated Equipment* **854** (2017) 70.

[14] T. Mineo et al., *The ASTRI Mini-Array calibration software system*, in *Proc. 38th ICRC*, PoS(ICRC2023)733, (Nagoya, Japan), 2023.